Applied Catalysis B: Environmental 333 (2023) 122777

Contents lists available at ScienceDirect

Applied Catalysis B: Environmental

journal homepage: www.elsevier.com/locate/apcatb

Activating Pt clusters for efficient removal of HCHO by modulating V^{n+} within V_xO_y support

Zeyi Guo [a], Xiuxian Zhao [a], Guozhu Chen [b,*], Zhen Yang [a], Tongyao Liu [a], Riming Hu [a,*], Xuchuan Jiang [a,c,**]

[a] Institute for Smart Materials & Engineering, University of Jinan, No. 336 Nanxinzhuang West Road, Jinan 250022, PR China
[b] School of Chemistry and Chemical Engineering, University of Jinan, No. 336 Nanxinzhuang West Road, Jinan 250022, PR China
[c] School of Materials Science and Engineering, University of Jinan, No. 336 Nanxinzhuang West Road, Jinan 250022, PR China

ARTICLE INFO

Keywords:
Vanadium oxides
Pt cluster
Metal-support interaction
Formaldehyde oxidation
Atomic layer deposition

ABSTRACT

The catalytic performance of Pt clusters towards formaldehyde (HCHO) oxidation was activated by tuning the valence of vanadium (V) element within a V_xO_y support. Through a facile but efficient solvothermal synthesis and heat-treatment process, the V valence can be precisely regulated from V^{4+} to V^{5+}. Subsequently, the HCHO catalytic oxidation rate of Pt/V_xO_y catalyst has dramatically increased from 0.0146 to 0.0294 mmol·h^{-1}·m^{-2} at 15 °C. The increased V valence has effectively accelerated the charge transfer from V_xO_y support to Pt cluster, and promoted the upshift of *d*-band center of the Pt element, leading to a low reduction temperature of Pt^{2+} to Pt^0 and high production of reactive adsorbed oxygen. This study provides a simple but feasible strategy to tune the valence of V element within V_xO_y and offers new insights for the study of other possible multivalent metal oxides used in different catalytic reactions.

1. Introduction

Formaldehyde (HCHO), as a major indoor air pollutant, is widely concerned due to its extensive sources and serious harmfulness [1–5]. In order to reduce indoor HCHO concentration, various kinds of strategies were developed to eliminate HCHO [6–10]. Although conventional physical absorption and ventilation were well-known to be efficient for HCHO elimination, unfortunately, the adsorbents were effective for only a short period due to their limited removal capacities, while the indoor HCHO removal efficiency was too low by ventilation method. In contrast, catalytic oxidation method is regarded as the most effective method because it can continuously and completely oxidize HCHO into water and carbon dioxide at room temperature.

In the field of HCHO catalytic oxidation, multivalent metal oxides have been used due to their abundant valence states and excellent redox ability [11–14]. To improve the catalytic activity, the multivalent metal oxides are usually incorporated with noble metals. Especially Pt, thanks to its high catalytic activity, is often supported on multivalent metal oxides for HCHO oxidation [15–19]. In these catalytic systems, the alteration of the metal valence state within metallic oxides often triggers changes in catalytic performances. For example, Ye et al. introduced Pt into Co_3O_4-NiO and found that the presence of low-valent Co can improve its HCHO oxidation catalytic activity [20]. Chen et al. found that Fe_2O_3/Pt catalyst exhibited enhanced catalytic activity towards HCHO elimination when the Fe^{2+}/Fe^{3+} value was increased within Fe_2O_3 support [21]. The high content of low-valent Mn within Pt/MnO_2 catalyst was also found to be conducive to improve its catalytic performance [22]. Although the correlation between the valence state within supports and the catalyst performance has been demonstrated in the literatures, a detailed research on the relationship between the valence state and their catalytic performance as well as the interaction between the metal oxides and Pt is still missing.

Vanadium oxide (V_xO_y), being one of the multivalent metal oxides, bears unique redox properties due to its variable valence states [23,24]. More importantly, V_xO_y has excellent oxygen-providing capacity [25], which is crucial for an oxidation reaction. These characteristics enable V_xO_y to exhibit high catalytic performance in many oxidation reactions. So far, V_xO_y-based catalysts have been applied in denitration [26], partial oxidative dehydrogenation of hydrocarbons [27], oxidative desulfurization [28], partial oxidation of alcohols [29] and so on. Due to

* Corresponding authors.
** Corresponding author at: Institute for Smart Materials & Engineering, University of Jinan, No. 336 Nanxinzhuang West Road, Jinan 250022, PR China.
E-mail addresses: chm_chengz@ujn.edu.cn (G. Chen), ism_hurm@ujn.edu.cn (R. Hu), ism_jiangxc@ujn.edu.cn (X. Jiang).

https://doi.org/10.1016/j.apcatb.2023.122777
Received 24 January 2023; Received in revised form 13 April 2023; Accepted 17 April 2023
Available online 19 April 2023

its unique properties, V_xO_y-based catalysts also show good catalytic performance in volatile organic compounds (VOCs) elimination, *e.g.,* complete oxidation of chlorobenzene [30], benzene [31] and toluene [32]. Ferreira et al. [33] loaded V species on Al_2O_3 for benzene elimination, and found that the high content of V^{4+} was beneficial to the catalytic process. In consideration of the diversity of VOCs, the development of V_xO_y-based HCHO oxidation catalyst is of great significance for the co-elimination of indoor multi-component VOCs. Unfortunately, the study of V_xO_y-based catalysts used in HCHO elimination has rarely been reported yet. Meanwhile, revealing the effect of V valence states on the catalytic performance also has an important instructive significance for the development of high-performance HCHO oxidation catalysts based on multivalent metal oxides.

In this study, we prepared sea urchin-like VO_2 microspheres by a hydrothermal method, and controlled experimental variables during the heat-treatment process to modulate V valence state, followed by the loading of Pt clusters by means of atomic layer deposition (ALD) method. Due to the numerous flaky structures on V_xO_y surface, Pt is stabilized with a small size of ~2 nm. The catalytic behaviors of the as-prepared Pt/V_xO_y microspheres as well as the effects of high-valent V on the catalytic activity, redox property and metal-support interaction are studied in detail by XPS, H_2-TPR, *in-situ* DRIFTS characterizations and DFT theoretical calculations. We found that there is a stronger interaction between Pt and V_xO_y with high-valent V, which is responsible for its superior catalytic activity. Obviously, this study can expand the application of multivalent metal oxides in HCHO oxidation reaction, and deepen the understanding of the catalytic reaction mechanism of V_xO_y based catalysts towards HCHO oxidation.

2. Section for experimentation

2.1. Materials

All the reactants are of analytical grade and were used without further purification. Isopropyl alcohol ($(CH_3)_2CHOH$) and ethanol (CH_3CH_2OH) were purchased from Sinopharm Chemical Reagent Co. Ltd. Vanadium pentoxide (V_2O_5) and oxalic acid ($H_2C_2O_4$) were purchased from Macklin. (Methylcyclopentadienyl)trimethylplatinum ($MeCpPtMe_3$) was purchased from J & K Chemical Co. Ltd.

2.2. Catalyst preparation procedures

The synthetic procedure of VO_2 microspheres was carried out according to the literature with minor modification [34]. In a typical procedure, 1.2 g V_2O_5 and 2.5 g oxalic acid were added into 40 mL deionized water and stirred in an 80 °C oil bath with reflux device until the system turned into a blue solution. After cooling down to room temperature, 3 mL of the as-prepared blue solution was added to 30 mL isopropyl alcohol and stirred evenly. Then the mixture was heated in an oven at 200 °C for 12 h. After centrifugation, washing with ethanol for three times and drying in vacuum at 40 °C, the VO_2 microsphere was obtained. To tune the valence state of vanadium, the as-prepared VO_2 microsphere was heat treated at 350 °C for 0.5, 1 or 2 h (ramping rate: 2 °C·min^{-1}), the obtained samples were denoted as 0.5h-V_2O_5, 1h-V_2O_5 and 2h-V_2O_5, respectively.

The ALD process was carried out in a hot-wall, closed chamber-type ALD reactor utilizing nitrogen as a carrier gas. The obtained catalysts were denoted as Pt/VO_2, 0.5h-Pt/V_2O_5, 1h-Pt/V_2O_5 and 2h-Pt/V_2O_5, respectively.

2.3. Characterizations

The crystal structures of the as-prepared samples were characterized by X-ray powder diffraction (XRD) on a Japan Rigaku Model SmartLabSE X-ray diffractometer. The structures and morphologies of the samples were studied by scanning electron microscope (SEM, Regulus 8100, Hitachi, Japan), and high resolution transmission electron microscope (HRTEM, JEOL, JEM 2100F) equipped with an annular dark-field detector and an energy dispersive X-ray spectrometer (EDS). The surface chemical valence states of the samples were characterized by X-ray photoelectron spectroscopy (XPS) with Al Kα radiation. The binding energies were calibrated with O 1s (530.0 eV) as the standard. The specific surface area was measured by the Brunauer-Emmett-Teller (BET) method using Micromeritics Tristar II 3020 instrument (test temperature: −196 °C). Before BET testing, all the samples were degassed at 120 °C for over 6 h (Ar atmosphere). The pore size distribution was determined by BJH method using N_2 adsorption data. Hydrogen temperature-programmed reduction (H_2-TPR) experiment was performed with a thermal conductivity detector on 100 mg sample in 80% (molar) argon and 20% (molar) hydrogen gas mixture (gas flow rate: 30 mL·min^{-1}, temperature ramp rate: 10 °C·min^{-1}). The loading amount of Pt in the samples was determined by ICP-OES conducted on ICAP7200. The *in-situ* DRIFTS characterization was performed on a Bruker Tensor II FT-IR spectrometer. A BaF_2 window was selected as the diffuse reflection cell of the *in-situ* diffuse infrared spectroscopic system. The *in-situ* DRIFTS characterization was carried out at 60 °C, the gas flow rate was 100 mL·min^{-1}. HCHO gas is generated by flowing N_2 through an aqueous HCHO solution in a 25 mL conical flask at 20 °C. The HCHO adsorption was carried out under HCHO/N_2 atmosphere. The O_2 purging was carried out under 20 vol% O_2/N_2 atmosphere. The *in-situ* reaction was carried out under HCHO/20 vol% O_2/N_2 atmosphere. Before the test, the samples were purified at 120 °C for 30 min under N_2 atmosphere.

2.4. Catalyst performance

Catalytic activity and stability were studied using a continuous flow fixed-bed micro-reactor at atmospheric pressure. In a typical procedure, the system was first purged with high purity N_2 gas and then a gas mixture of HCHO/O_2/N_2 (HCHO concentration: ~240 ppm, H_2O concentration: ~1000 ppm, O_2 content: ~20 vol%) was introduced into the reactor. The amount of catalyst was 100 mg. The seed gas flow rate was 125 mL·min^{-1}, corresponding to a GHSV (gas hourly space velocity) of 75,000 mL·h^{-1}·g^{-1}. Gas samples were analyzed with a Multi-Gas Analyzer (DKG-ONE, Duke Technology, China) based on photoacoustic infrared spectrum. The HCHO conversion was calculated using the following equation:

$$\text{Conversion}(\%) = \frac{[\text{HCHO}]_{\text{in}} - [\text{HCHO}]_{\text{out}}}{[\text{HCHO}]_{\text{in}}} \times 100\%$$

where $[\text{HCHO}]_{\text{in}}$ and $[\text{HCHO}]_{\text{out}}$ were the HCHO concentration in the inlet and outlet, respectively.

3. Results and discussion

3.1. Characterizations of V_xO_y and Pt/V_xO_y catalysts

The morphology of the as-prepared samples is characterized using SEM technique. As shown in Fig. 1, the VO_2 microspheres (the particle size is ~2 μm) display a spherical sea urchin-like morphology with an array composed of nanosheets and/or nanorods on the surface. After heat-treatment at 350 °C in air, almost no changes in morphologies and size are observed. Even the calcination time was extended to 2 h, the array structure can still be well maintained.

The crystal structures of the obtained samples are characterized by XRD. As shown in Fig. 2, the XRD pattern of the as-prepared VO_2 microspheres is consistent with the reported result [34], which is determined as monoclinic VO_2 phase with the lattice parameters of a = 4.5968 Å, b = 5.6844 Å, c = 4.9133 Å, β = 89.39° (Fig. 2a). When it was treated at 350 °C for 0.5 h, all the diffraction peaks of the obtained sample are indexed to V_2O_5 (JCPDS no.41-1426). It is noted that the

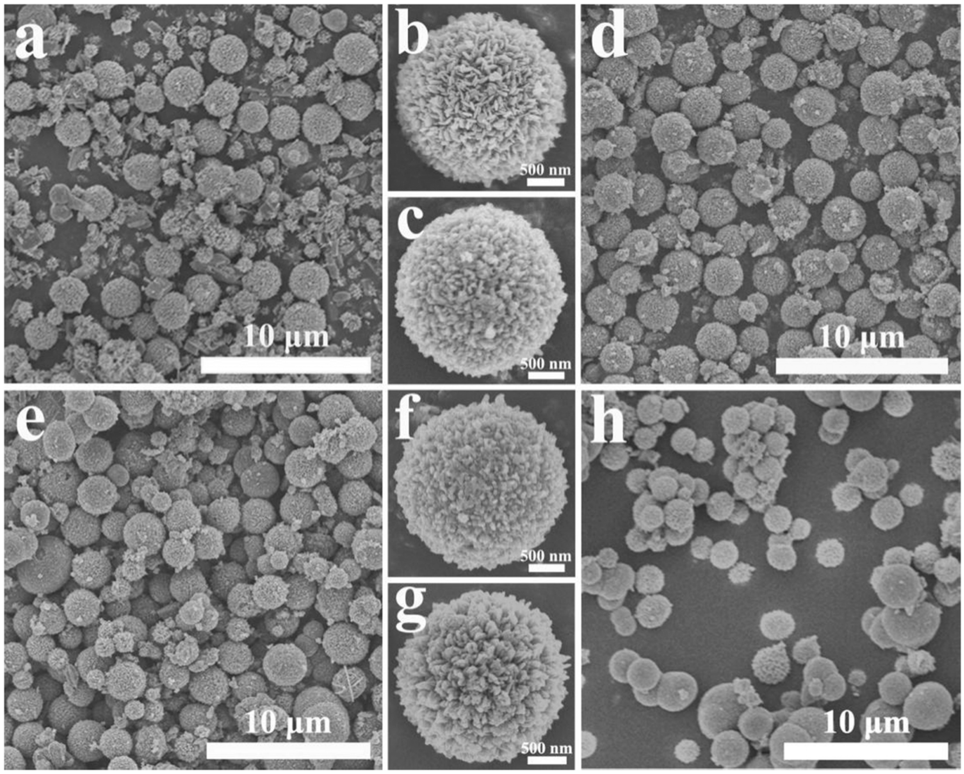

Fig. 1. SEM images of (a, b) VO_2, (c, d) 0.5h-V_2O_5, (e, f) 1h-V_2O_5 and (g, h) 2h-V_2O_5 microspheres.

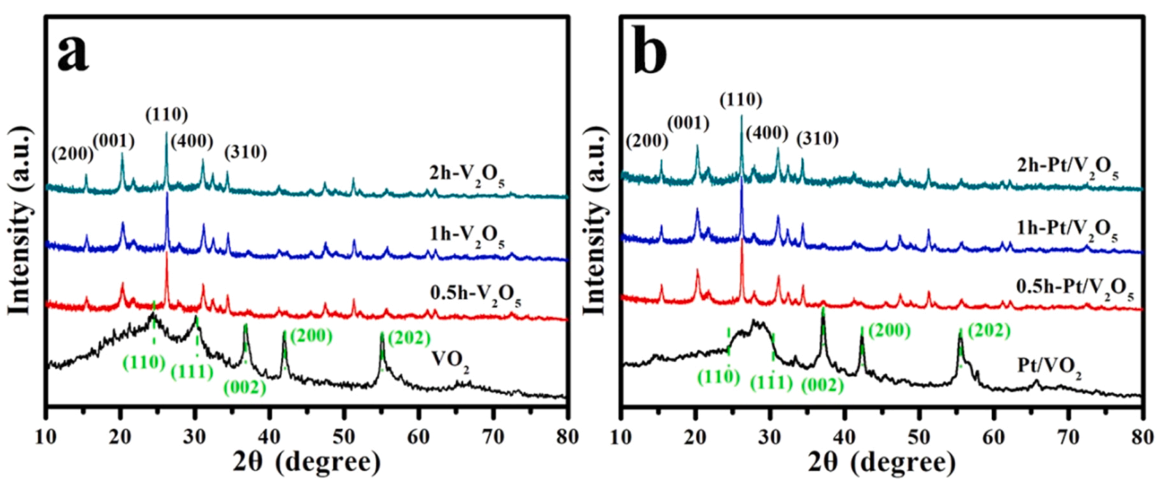

Fig. 2. XRD patterns of (a) VO_2, 0.5h-V_2O_5, 1h-V_2O_5, 2h-V_2O_5 and (b) Pt/VO_2, 0.5h-Pt/V_2O_5, 1h-Pt/V_2O_5, 2h-Pt/V_2O_5 microspheres.

diffraction peaks of VO_2 disappear, indicating that VO_2 can be converted into V_2O_5 under this condition. When the calcination time was extended to 1, 2 h, there is no obvious difference in XRD pattern. After loading Pt by ALD method, there is a major change for the diffraction peaks located in the range of 10–35°. Considering the complexity and variability of VO_2 crystal structure, this phenomenon should be ascribed to the high temperature condition (270 °C) during the Pt deposition process, which leads to the partial transformation of the VO_2 crystal phase. In the case of V_2O_5 support, there are no obvious changes for XRD diffraction peaks after Pt deposition (Fig. 2b). In addition, there are no characteristic peaks of Pt species, suggesting the highly dispersed and/or small particle size of Pt species [35].

The specific surface area has always been considered as an important factor affecting the performance of catalysts. Hence, the specific surface areas of the as-prepared catalysts are measured and shown in Fig. S1. The N_2 adsorption-desorption isotherms of the as-prepared catalysts display type-III behavior with a type-H3 hysteresis loop. Based on the isotherms (Fig. S1a), the BET surface areas are calculated (VO_2: 9.6 $m^2 \cdot g^{-1}$, 0.5h-V_2O_5: 17.7 $m^2 \cdot g^{-1}$, 1h-V_2O_5: 19.0 $m^2 \cdot g^{-1}$, 2h-V_2O_5: 15.2 $m^2 \cdot g^{-1}$). Compared with that of VO_2, the BET surface areas of the V_2O_5 samples increase obviously, possibly due to the removal of residua in VO_2 channels. After loading Pt, the BET surface areas of the samples increased slightly (Pt/VO_2: 14.9 $m^2 \cdot g^{-1}$, 0.5h-Pt/V_2O_5: 22.2 $m^2 \cdot g^{-1}$, 1h-Pt/V_2O_5: 21.0 $m^2 \cdot g^{-1}$, 2h-Pt/V_2O_5: 16.4 $m^2 \cdot g^{-1}$), which was attributed to the incomplete occupation of the support channels by Pt species (Fig. S1b). The BJH pore diameter of all samples is concentrated at ~3 nm, indicating the calcination and ALD processes have no substantial effect on the pore size.

3.2. The effect of surface element valence on catalyst activity

These four catalysts with the similar morphology and specific surface area were investigated to evaluate their catalytic performance toward HCHO oxidation. The loading amount of Pt were determined as 2.57 wt %, 1.05 wt%, 1.12 wt% and 1.73 wt% for Pt/VO_2, 0.5h-Pt/V_2O_5, 1h-Pt/V_2O_5 and 2h-Pt/V_2O_5 catalysts, respectively. As shown in Fig. 3a, the initial HCHO conversion of Pt/VO_2 catalyst is ~22% at 50 °C, and the conversion remains at ~16% after continuous reaction for 1 h. When VO_2 was treated at 350 °C, the catalytic activities of Pt/V_2O_5 catalysts were significantly improved. Specifically, the initial HCHO conversion of 0.5h-Pt/V_2O_5 catalyst is ~41% and remains at ~36% after continuous reaction for 1 h. For 1h-Pt/V_2O_5 and 2h-Pt/V_2O_5 catalysts, the initial conversion is increased to ~46%, which can maintains above 41% after 1 h reaction. Considering that calcination time may relate to the content of high-valent V, the as-prepared samples were tested by XPS. As shown in Fig. S2, there are two main oxygen species, including lattice oxygen (~530.0 eV, O_{latt}) and surface adsorbed oxygen (~531.3 eV, O_{ads}), for the samples without Pt loading [36,37]. The content of O_{ads} is expressed as the ratio of the O_{ads} peak area to the sum of the peak areas of O_{ads} and O_{latt}, and it decreases gradually with the prolonging of treatment time (Table S1). V mainly exists in the form of V^{4+} (~516.0 eV) and V^{5+} (~517.3 eV) [38,39]. The content of V^{5+} is calculated by the ratio of the V^{5+} peak area to the total peak area of V^{4+} and V^{5+}, and it gradually increases with the extension of calcination time (Table S1). After loading of Pt, the valence states of V^{4+} and V^{5+} are also identified in Pt/VO_2, 0.5h-Pt/V_2O_5, 1h-Pt/V_2O_5 and 2h-Pt/V_2O_5 catalysts, and the contents of V^{5+} do not change significantly compared with the ones within individual support (Fig. 3b). Interestingly, the catalytic activity is positively related to the content of V^{5+}. As shown in Fig. S5, the reaction rates ($R_{s\text{-}catal}$) are gradually improved with the increase of V^{5+} contents. For the O 1s spectra (Fig. 3c), the content of O_{ads} in Pt/VO_2, 0.5h-Pt/V_2O_5, 1h-Pt/V_2O_5 and 2h-Pt/V_2O_5 catalysts are 0.360, 0.430, 0.457 and 0.497, respectively. The order of the O_{ads} contents is reversed between individual V_xO_y and Pt/V_xO_y. For VO_2 sample, the content of O_{ads} is as high as 0.490. This phenomenon should be attributed to the instability of VO_2, which results in the adsorption of a large number of non-reactive oxygen species on its surface. During ALD process, high temperature will lead to desorption of the non-reactive oxygen species. The 2h-Pt/V_2O_5 catalyst has the highest O_{ads} content. Generally, stronger metal-support interaction is more conducive to the generation of reactive O_{ads}. For the Pt 4f spectra (Fig. 3d), Pt mainly exists in the form of Pt^0 (~69.0 eV), Pt^{2+} (~71.7 eV) and Pt^{4+} (~72.9 eV) [40,41]. The content of different valence Pt is also calculated by the ratio of peak area. The content of Pt^0 in the catalysts is very low, thus we put our emphasis on Pt^{2+} since Pt^{2+} is generally considered to be beneficial to HCHO oxidation [42,43]. The 2h-Pt/V_2O_5 catalyst contains the highest content of Pt^{2+}, which is one of the reasons for its best catalytic activity. It should be noted that the reactive O_{ads} are considered to be the active species for HCHO oxidation [44,45]. And the $R_{s\text{-}catal}$ is also positively correlated with the content of O_{ads} in this work (Fig. S5). Although the Pt^{2+} content of Pt/VO_2 catalyst is also considerable, its O_{ads} content is the lowest, which leads to its worst catalytic activity. As stated above, Pt^{2+} and reactive O_{ads} should be the main active species for the catalytic oxidation of HCHO.

In order to further identify the HCHO elimination ability of the catalysts, Pt/VO_2 and 2h-Pt/V_2O_5 catalysts are selected for further characterizations. As shown in Fig. 4a, the HCHO conversion of 2h-Pt/

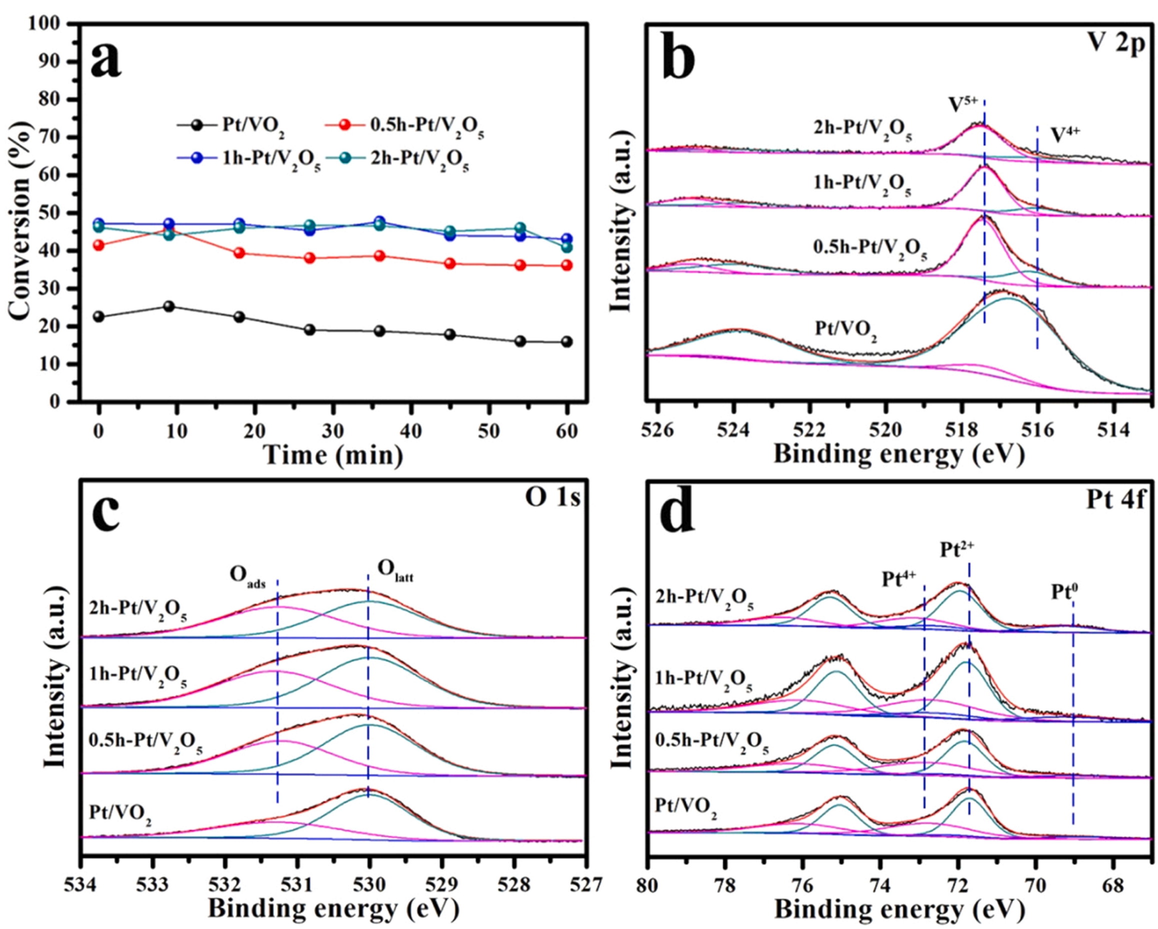

Fig. 3. (a) HCHO conversion as a function time at 50 °C for Pt/VO_2, 0.5h-Pt/V_2O_5, 1h-Pt/V_2O_5 and 2h-Pt/V_2O_5 microspheres; and XPS of Pt/VO_2, 0.5h-Pt/V_2O_5, 1h-Pt/V_2O_5 and 2h-Pt/V_2O_5 microspheres ((b) V 2p, (c) O 1s, (d) Pt 4f).

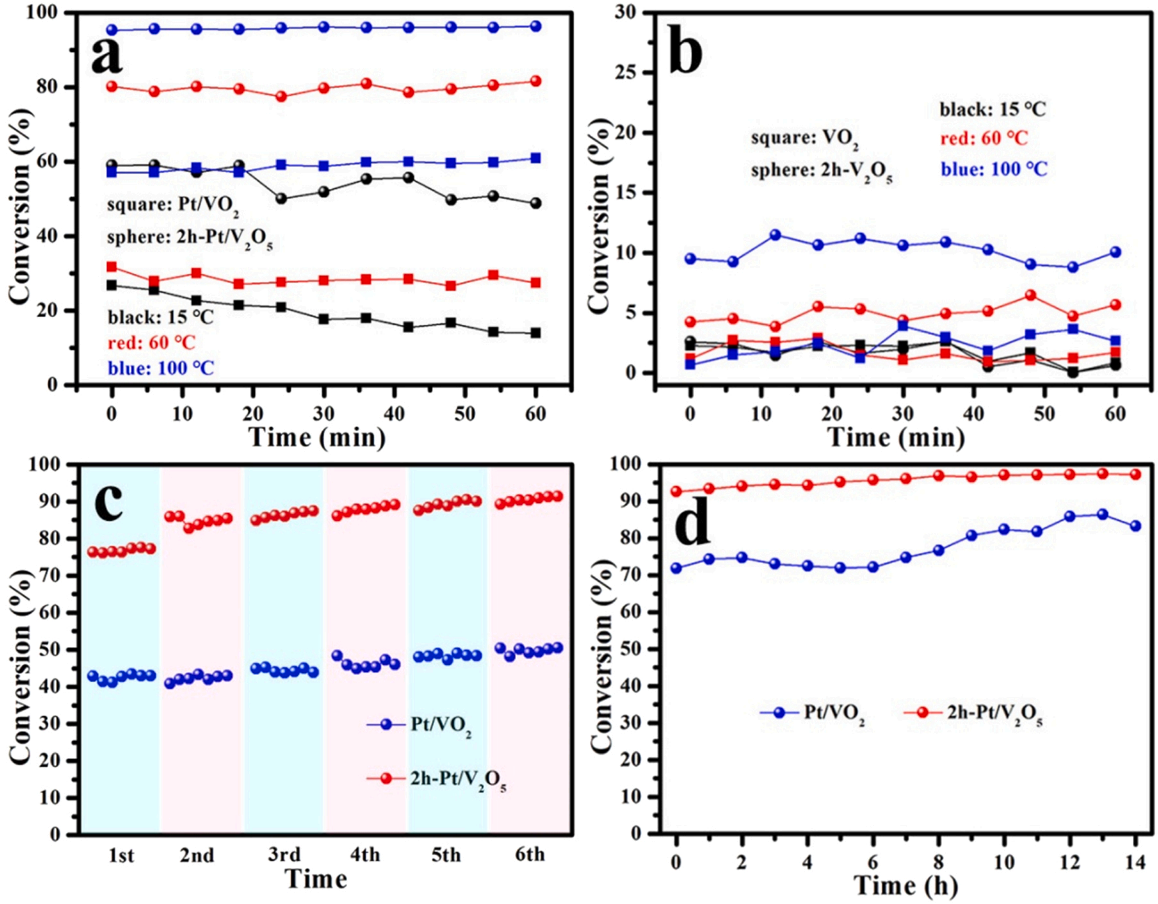

Fig. 4. HCHO conversion as a function time at a certain temperature for (a) Pt/VO_2, 2h-Pt/V_2O_5 and (b) VO_2, 2h-V_2O_5 microspheres; (c) cycle performance test and (d) long-term test of Pt/VO_2 and 2h-Pt/V_2O_5 catalysts.

V_2O_5 catalyst is up to ~60% at 15 °C, and the conversion can still be maintained at ~50% after continuous reaction for 1 h. However, for Pt/VO_2 catalyst, the HCHO conversion at 15 °C is only ~27%, and it decreases to ~14% after 1 h reaction. At 60 °C, the HCHO conversion gap between Pt/VO_2 and 2h-Pt/V_2O_5 catalysts is as high as ~49%. Even at 100 °C, the HCHO conversion of 2h-Pt/V_2O_5 catalyst reaches ~96%, there is still ~39% conversion gap between the two catalysts. The stability of the two catalysts was also tested. Although the activities will be inhibited due to the covering of active sites by intermediates after 1 h operation at low temperature, both catalysts have good cyclic performance and long-term stability under full-load operation. As shown in Fig. 4c, d, the catalytic activity of the two catalysts was even improved after cycle performance test and long-term test, and their structure can be maintained well after a long-term test (Table S2). Encouragingly, compared with the reported HCHO oxidation catalysts, the as-prepared catalysts in this work still has significant advantages in catalytic activity (Table S3). In the absence of Pt species, 2h-V_2O_5 catalyst still has better HCHO elimination property than VO_2 catalyst (Fig. 4b). These phenomena fully explain the superior catalytic property of high-valent V_xO_y for HCHO oxidation.

To determine whether the element valence states and structures of the catalysts changed before and after catalysis, the samples that undergo catalysis are tested by XPS and XRD (as shown in Fig. S4 and Fig. S3). After catalysis, V^{4+} and V^{5+} still exist in the samples and the content of V^{5+} has no obvious change, indicating that V_xO_y microspheres can remain stable during the catalytic process. At the same time, the content of O_{ads} in Pt/VO_2 catalyst increased slightly, while it decreased significantly for 2h-Pt/V_2O_5 catalyst. Combined with the above results, the content of O_{ads} in 2h-V_2O_5 is much lower than that in VO_2, but the catalytic activity of 2h-V_2O_5 is significantly higher. These fully prove that the O_{ads} in the high-valent V_xO_y are more active than those in the low-valent V_xO_y, and it will be consumed during the catalytic reaction. For the Pt species, the content of Pt^{2+} in the two catalysts remains stable. Notably, after catalytic test and long-term test (Fig. S4), the Pt 4f peaks of 2h-Pt/V_2O_5 catalyst shifted obviously to a low binding energy direction, which indicates that V_2O_5 can transfer more electrons to Pt during the HCHO oxidation reaction. Meanwhile, the XRD diffraction peaks (Fig. S3) of the two catalysts have almost no changes before and after catalysis. In short, the two catalysts can maintain structural stability in the catalytic process.

3.3. Element distribution and redox capacity analysis

The morphology and composition are characterized using SEM and HRTEM techniques. As shown in Fig. 5a, d, the two catalysts still maintain the microsphere structure. The interlayer spacings of Pt/VO_2 measured in the HRTEM images are ~0.37 and ~0.23 nm, which can be indexed as (01−1) crystal planes of VO_2 and (111) crystal planes of Pt species, respectively (Fig. 5b). For 2h-Pt/V_2O_5 catalyst, the interlayer spacings attributed to (200) crystal planes of V_2O_5 (~0.58 nm) and (111) crystal planes of Pt species are observed (Fig. 5e). These further confirmed the presence of Pt species and determined the crystalline phases of VO_2 and V_2O_5. By measurement, Pt species in Pt/VO_2 and 2h-Pt/V_2O_5 catalysts exist in the form of clusters and have similar particle sizes of 2.0 and 2.4 nm, respectively. And the elemental-mapping images show that V, O and Pt are uniformly distributed in the two catalysts (Fig. 5c, f). This indicates that the element distribution state and the size of Pt clusters are not responsible for the performance disparity between

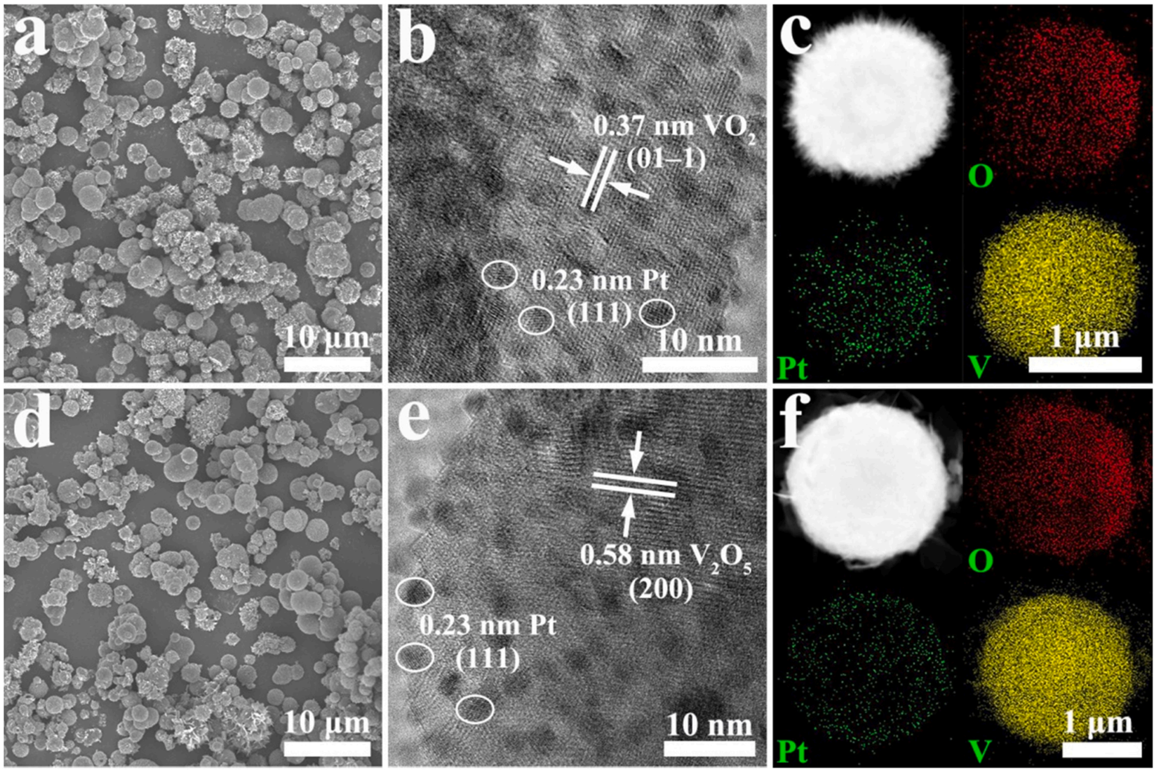

Fig. 5. (a) SEM, (b) HRTEM, (c) HAADF-STEM and elemental-mapping images of Pt/VO_2, and (d-f) the images corresponding to 2h-Pt/V_2O_5.

the two catalysts.

The redox capacity of the catalysts greatly affects its catalytic performance. Here, the redox capacities of the catalysts are characterized by H_2-TPR. As shown in Fig. 6, pure VO_2 only has a reduction peak at ~643 °C, which should be attributed to the reduction of V^{4+} to V^{3+} [46]. By contrast, 2h-V_2O_5 has two reduction peaks above 650 °C, which belong to the reduction of V^{5+} to V^{4+} and V^{4+} to V^{3+}, respectively [47,48]. After loading Pt by ALD method, two broad peaks of Pt/VO_2 catalyst appear at 70–325 °C and 325–500 °C. Among them, the broad peak at 70–325 °C is attributed to the reduction of oxidized Pt and surface adsorbed oxygen [22,47], and the peak at 325–500 °C belongs to the reduction of surface VO_2. The 2h-Pt/V_2O_5 catalyst shows reduction peaks at 50–300 °C and 350–500 °C, the peaks at 50–300 °C are ascribed to the reduction of oxidized Pt and surface adsorbed oxygen, the peak at 350–500 °C is related to the reduction of surface V_2O_5.

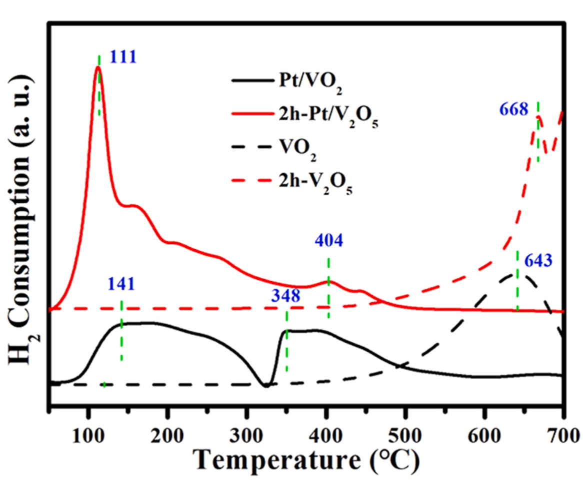

Fig. 6. H_2-TPR of VO_2, 2h-V_2O_5, Pt/VO_2 and 2h-Pt/V_2O_5 catalysts.

Compared with the samples without Pt, the reduction peaks of V species in the two catalysts are significantly shifted to the low temperature direction, indicating that there is a strong metal-support interaction between Pt and V_xO_y, thus promoting the reduction of V species. Meanwhile, the reduction temperatures of Pt and surface adsorbed oxygen species in 2h-Pt/V_2O_5 catalyst are obviously lower than that in Pt/VO_2, which indicates that the metal-support interaction in 2h-Pt/V_2O_5 catalyst is stronger than Pt/VO_2 catalyst. Stronger interaction generally promotes the emergence of more reactive O_{ads} and Pt^{2+}, which is beneficial to the enhancement of catalytic activity and is consistent with XPS results.

3.4. Catalytic reaction mechanism of HCHO oxidation

In-situ DRIFTS is used to study the possible reaction mechanism of HCHO oxidation on Pt/V_xO_y catalysts. As shown in Fig. 7, the characteristic peaks of molecularly adsorbed HCHO (~1006, ~1056 cm^{-1}), intermediates such as dioxymethylene (DOM: ~1035, ~1405, ~2797 cm^{-1}), formate species (~1771, ~2860, ~2898 cm^{-1}) and CO bridge adsorbed on Pt clusters (Pt-CO-Pt: ~1745 cm^{-1}), final products *e.g.,* H_2O (~1640 cm^{-1}) and CO_2 (~1455 cm^{-1}), OH groups (~3049–3659 cm^{-1}) are all observed during the HCHO oxidation process [17,44,49–51]. In the “HCHO adsorption” process (Fig. 7a, b), the characteristic peaks of OH groups and final products such as CO_2 (~1455 cm^{-1}) and H_2O (~1640 cm^{-1}) are observed in 2h-Pt/V_2O_5 catalyst at 10 min. Their intensity gradually increases with time and reaches saturation at 30 min. But for Pt/VO_2 catalyst, the peaks of CO_2 and H_2O appear after 25 min, and the intensities are still weak at 30 min. At the same time, a strong signal of DOM (~1405 cm^{-1}) is observed in Pt/VO_2 catalyst. These indicate that the adsorbed HCHO can be completely oxidized by reactive O_{ads} species on the surface of 2h-Pt/V_2O_5 catalyst, but it is difficult on that of Pt/VO_2. No adsorption peaks of HCHO molecule are observed on the two catalysts, which are attributed to the degradation of HCHO molecules by the surface oxygen species of the two catalysts. When O_2 is introduced to purge (Fig. 7c, d),

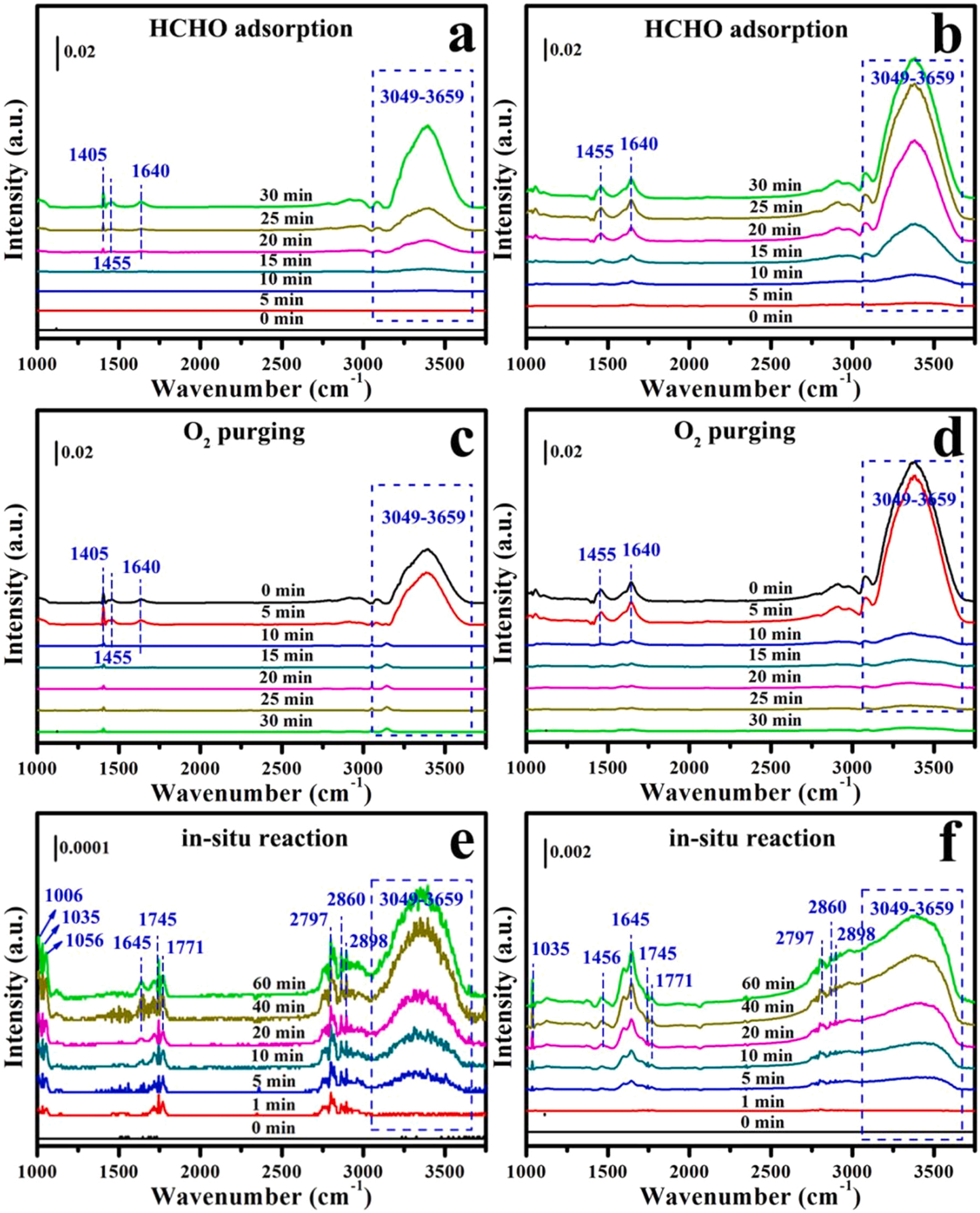

Fig. 7. *In-situ* DRIFTS of Pt/VO_2 and 2h-Pt/V_2O_5 catalysts. HCHO adsorption, O_2 purging and *in-situ* reaction process of (a, c, e) Pt/VO_2 and (b, d, f) 2h-Pt/V_2O_5, respectively.

the characteristic peaks of OH groups and final products in the two catalysts decreased rapidly, and disappeared completely after purging for 30 min. However, the characteristic peak of DOM can still be observed in Pt/VO_2 catalyst, which confirms that O_2 is difficult to be activated to convert intermediates into final products on Pt/VO_2 catalyst. In the "*in-situ* reaction" mode (Fig. 7e, f), the strong characteristic peaks of HCHO and intermediates can still be observed in Pt/VO_2 catalyst, and the characteristic peak of CO_2 is missing, which further proves the weak HCHO elimination ability of Pt/VO_2 catalyst. Compared with Pt/VO_2 catalyst, there are stronger signals of final products and weaker signals of intermediate products in 2h-Pt/V_2O_5 catalyst, and no peak of HCHO molecule appears. Obviously, 2h-Pt/V_2O_5 catalyst has better HCHO elimination activity. This better HCHO elimination activity should come from the stronger interaction between Pt and V_2O_5. Based on the above discussion, the HCHO oxidation mechanism was clarified: HCHO molecules are attacked by reactive oxygen species (reactive O_{ads} and/or activated O_2) followed by converting into DOM and formate species, and then further converted into H_2O and CO. Finally, CO reacts with reactive oxygen species to generate CO_2.

3.5. DFT studies on the different catalytic properties of Pt/VO_2 and Pt/V_2O_5 for HCHO oxidation

To gain further insight into the origin of high catalytic activities of Pt/V_2O_5, DFT calculations were further carried out. Firstly, Pt_{10} cluster, which is widely employed as the theoretical model for Pt cluster [52,53], are loaded on VO_2 and V_2O_5 to simulate Pt/VO_2 and Pt/V_2O_5. Then, the reaction energy barriers from HCHO to CO_2 on above two catalysts are calculated (Fig. 8).

One can see that the adsorption energy (E_{ad}) of HCHO on Pt/V_2O_5 ($E_{ad} = -1.43$ eV) is more negative than that on Pt/VO_2 ($E_{ad} = -0.64$ eV), which indicates a higher HCHO capture capability for Pt/V_2O_5. From this point of view, Pt/V_2O_5 can also be served as the HCHO capture material. More important, it can be found that Pt/V_2O_5 possess a higher catalytic activity than Pt/VO_2 due to a lower reaction energy barrier (Fig. 8), which confirms previous experimental results. Specifically, the highest energy barriers from HCHO to CO_2 and H_2O are 1.98 eV on Pt/VO_2, indicating its lower catalytic activity. By comparison, the interaction between Pt and V_2O_5 can significantly improve the catalytic activity, in which the reaction processes can be completed only by overcoming an lower energy barrier of 0.71 eV (the configurations of reaction intermediates on Pt/V_2O_5 are shown in Fig. 8). Compared with Pt/V_xO_y catalysts, HCHO oxidation reaction on V_xO_y catalysts needs to overcome a higher energy barrier (Fig. S6). And the energy barrier on V_2O_5 catalyst is also lower than that on VO_2 catalyst.

The calculated project density of states of Pt-d orbital in Pt/V_2O_5 and Pt/VO_2 are shown in Fig. 9a. It can be found that the *d*-band center (ε_d) of Pt/V_2O_5 ($\varepsilon_d = -0.62$ eV) is closer to the Fermi level than that of Pt/VO_2 ($\varepsilon_d = -0.71$ eV). Previous reports showed that the ε_d of catalysts determines their adsorption and catalytic activity, where improvement of catalytic activity always accompanied with a higher position of ε_d [54–56]. Therefore, the origin of the enhanced catalytic activity of Pt/V_2O_5 can be attributed to the upward shift of the ε_d of Pt atoms. Fig. 9b and c show the calculated charge density difference of Pt/V_2O_5 and Pt/VO_2, 1.19 (0.70) e^- are transferred from V_2O_5 (VO_2) to Pt cluster. On one hand, it indicates a stronger metal-supports interaction for Pt/V_2O_5 compared with Pt/VO_2. On the other hand, significant charge transfer behavior can increase the electrons number around the Fermi level, subsequently, the catalytic activity can be improved.

4. Conclusions

This study has developed a simple but effective method to prepare V_xO_y and Pt modified V_xO_y microspheres with different vanadium valence states (V^{n+}) by controlling the pertinent variable. Following by testing and characterizing the obtained V_xO_y and Pt/V_xO_y microspheres in electronic transfer and the corresponded catalytic performance in HCHO oxidation, a few interesting results and findings can be summarized and demonstrated, as below:

i) Pt/V_xO_y catalysts have shown exemplary catalytic activity in HCHO oxidation reaction at room temperature, and the catalytic activity can be significantly improved by tuning the V valence state, among them, 2h-Pt/V_2O_5 catalyst exhibited the highest catalytic activity;
ii) The O_{ads} reactivity in high-valent V_xO_y (V_2O_5) is higher than that in low-valent V_xO_y (VO_2), because the low-valent one is unstable in the air and tends to absorb more inactive O_{ads} which can be desorbed by heating process;
iii) The good electron transport capacity of V_xO_y to noble-metal Pt leads to a strong metal-support interaction between Pt and V_xO_y microspheres, and promotes the reduction of V_xO_y greatly.
iv) The interaction of Pt/V_2O_5 is stronger than that of Pt/VO_2, and the electron transport capacity of V_2O_5 to Pt is also stronger than that of VO_2 to Pt, resulting in higher concentration of reactive O_{ads} and Pt^{2+} species, as well as leading to Pt clusters more active in HCHO oxidation reaction.

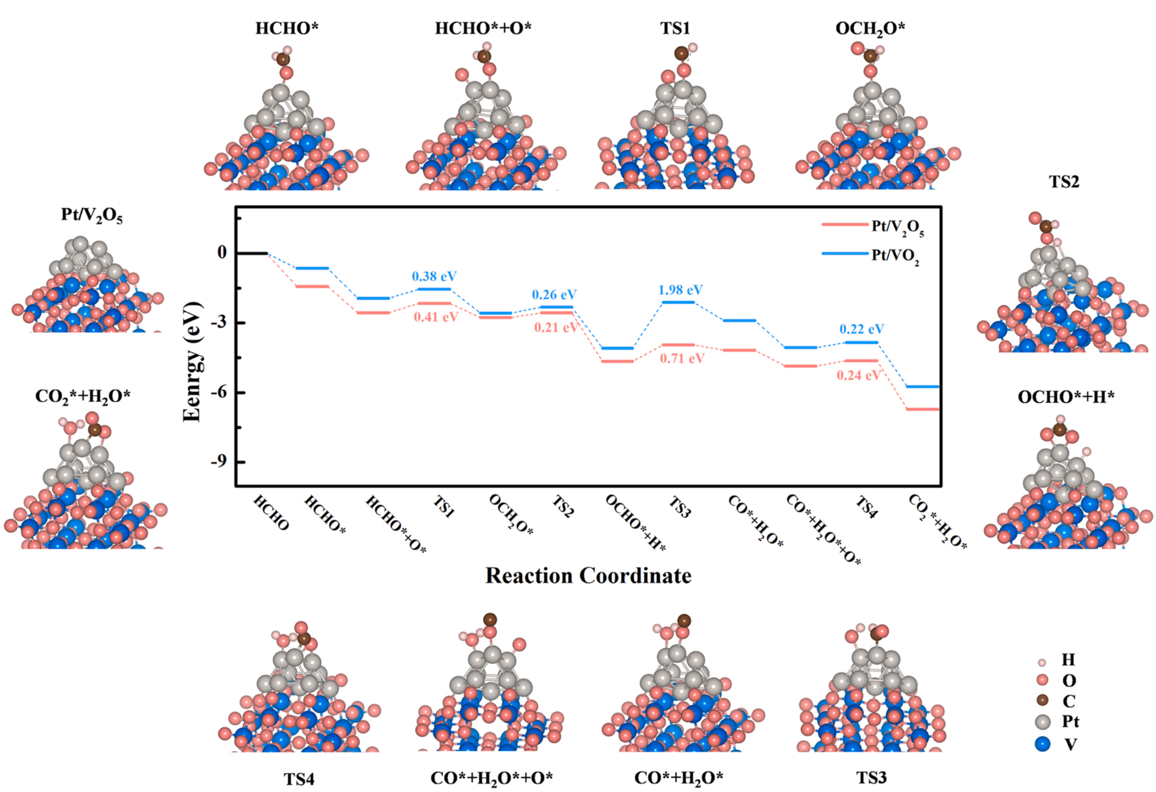

Fig. 8. The calculated reaction energy barriers of HCHO oxidation reaction on Pt/V_2O_5 and Pt/VO_2. Inserts are the configurations of reaction intermediates on Pt/V_2O_5.

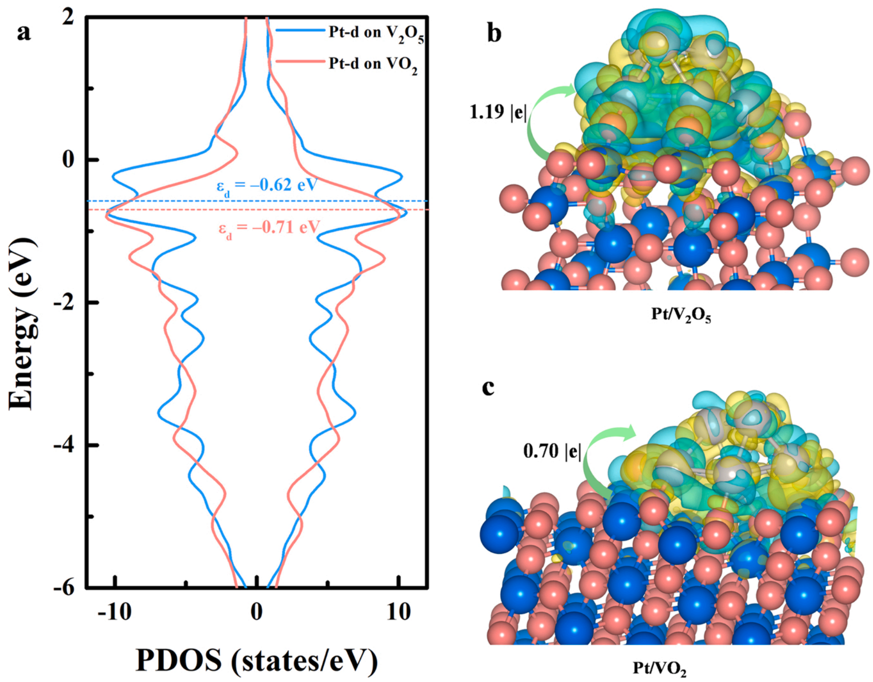

Fig. 9. Electronic structures analysis. (a) Project density of states (PDOS) of Pt-d orbital in Pt/V_2O_5 and Pt/VO_2. The charge density difference of (b) Pt/V_2O_5 and (c) Pt/VO_2, the isovalue of the isosurfaces is 2.0×10^{-3} eÅ^{-3}, yellow and cyan represents the charge accumulation and deletion, respectively.

This work not only expands the application of V_xO_y-based catalysts, but also provides guidance for the preparation of highly active multivalent metal oxides-based HCHO oxidation catalysts.

CRediT authorship contribution statement

Zeyi Guo: Conceptualization, Methodology, Investigation, Writing. **Xiuxian Zhao:** Data curation. **Guozhu Chen:** Supervision, Conceptualization. **Zhen Yang:** Investigation. **Tongyao Liu**: Reviewing. **Riming Hu:** Resources, Visualization. **Xuchuan Jiang:** Writing – review & editing, Funding acquisition, Project administration.

Declaration of Competing Interest

The authors declare that they have no known competing financial interests or personal relationships that could have appeared to influence the work reported in this paper.

Data Availability

Data will be made available on request.

Acknowledgment

The authors acknowledge the financial support from the National Natural Science Foundation of China (Grant No. 21878121), Jinan Science and Technology Bureau (2021GXRC086), the financial support from the Shandong Provincial Natural Science Foundation (Grant No. ZR202102230042).

Appendix A. Supporting information

Supplementary data associated with this article can be found in the online version at doi:10.1016/j.apcatb.2023.122777.

References

[1] W. Wei, C. Howard-Reed, A. Persily, Y. Zhang, Standard formaldehyde source for chamber testing of material emissions: model development, experimental evaluation, and impacts of environmental factors, Environ. Sci. Technol. 47 (2013) 7848–7854.
[2] D. Bourdin, P. Mocho, V. Desauziers, H. Plaisance, Formaldehyde emission behavior of building materials: on-site measurements and modeling approach to predict indoor air pollution, J. Hazard. Mater. 280 (2014) 164–173.
[3] J.L. Shie, C.H. Lee, C.S. Chiou, C.T. Chang, C.C. Chang, C.Y. Chang, Photodegradation kinetics of formaldehyde using light sources of UVA, UVC and UVLED in the presence of composed silver titanium oxide photocatalyst, J. Hazard. Mater. 155 (2008) 164–172.
[4] T. Salthammer, S. Mentese, R. Marutzky, Formaldehyde in the indoor environment, Chem. Rev. 110 (2010) 2536–2572.
[5] W.W. Guo, Z. Luo, H.J. Lv, C.L. Hill, Aerobic oxidation of formaldehyde catalyzed by polyvanadotungstates, ACS Catal. 4 (2014) 1154–1161.
[6] R. Ojani, J.B. Raoof, E. Zarei, Photoelectrocatalytic oxidation of formaldehyde using a Ti/TiO_2 foil electrode. Application for its novel and simple photoelectrochemical determination, Talanta 99 (2012) 277–282.
[7] B.Y. Bai, Q. Qiao, J.H. Li, J.M. Hao, Progress in research on catalysts for catalytic oxidation of formaldehyde, Chin. J. Catal. 37 (2016) 102–122.
[8] G. de Falco, M. Barczak, F. Montagnaro, T.J. Bandosz, A new generation of surface active carbon textiles as reactive adsorbents of indoor formaldehyde, ACS Appl. Mater. Inter. 10 (2018) 8066–8076.
[9] H.L. Dou, D. Long, X. Rao, Y.P. Zhang, Y.M. Qin, F. Pan, K. Wu, Photocatalytic degradation kinetics of gaseous formaldehyde flow using TiO_2 nanowires, ACS Sustain. Chem. Eng. 7 (2019) 4456–4465.
[10] S. Wang, K. Han, Z. Deng, F. Wang, CeO_2 nanorods decorated with Pt nanoparticles as catalysts for oxidative elimination of formaldehyde, ACS Appl. Nano Mater. 5 (2022) 10036–10046.
[11] B.Y. Bai, H. Arandiyan, J.H. Li, Comparison of the performance for oxidation of formaldehyde on nano-Co_3O_4, 2D-Co_3O_4, and 3D-Co_3O_4 catalysts, Appl. Catal. B-Environ. 142 (2013) 677–683.
[12] Y.C. Huang, B. Long, M.N. Tang, Z.B. Rui, M.S. Balogun, Y.X. Tong, H.B. Ji, Bifunctional catalytic material: an ultrastable and high-performance surface defect CeO_2 nanosheets for formaldehyde thermal oxidation and photocatalytic oxidation, Appl. Catal. B-Environ. 181 (2016) 779–787.
[13] H.C. Wang, W.Q. Guo, Z. Jiang, R.O. Yang, Z. Jiang, Y. Pan, W.F. Shangguan, New insight into the enhanced activity of ordered mesoporous nickel oxide in formaldehyde catalytic oxidation reactions, J. Catal. 361 (2018) 370–383.
[14] B.B. Chen, B. Wu, L.M. Yu, M. Crocker, C. Shi, Investigation into the catalytic roles of various oxygen species over different crystal phases of MnO_2 for C_6H_6 and HCHO oxidation, ACS Catal. 10 (2020) 6176–6187.
[15] N.H. An, Q.S. Yu, G. Liu, S.Y. Li, M.J. Jia, W.X. Zhang, Complete oxidation of formaldehyde at ambient temperature over supported Pt/Fe_2O_3 catalysts prepared by colloid-deposition method, J. Hazard. Mater. 186 (2011) 1392–1397.

[16] Z.X. Yan, Z.H. Xu, B. Cheng, C.J. Jiang, Co_3O_4 nanorod-supported Pt with enhanced performance for catalytic HCHO oxidation at room temperature, Appl. Surf. Sci. 404 (2017) 426–434.
[17] S.Y. Huang, B. Cheng, J.G. Yu, C.J. Jiang, Hierarchical Pt/MnO_2-Ni$(OH)_2$ hybrid nanoflakes with enhanced room-temperature formaldehyde oxidation activity, ACS Sustain. Chem. Eng. 6 (2018) 12481–12488.
[18] S. Wang, Y. Wang, F.G. Wang, Room temperature HCHO oxidation over the Pt/CeO_2 catalysts with different oxygen mobilities by changing ceria shapes, Appl. Catal. A-Gen. 630 (2022), 118469.
[19] J. Xie, S. Wang, K. Zhao, M. Wu, F. Wang, Regulating the Pt-MnO_2 interaction and interface for room temperature formaldehyde oxidation, Inorg. Chem. 62 (2023) 904–915.
[20] J.W. Ye, B. Cheng, J.G. Yu, W.K. Ho, S. Wageh, A.A. Al-Ghamdi, Hierarchical Co_3O_4-NiO hollow dodecahedron-supported Pt for room-temperature catalytic formaldehyde decomposition, Chem. Eng. J. 430 (2022), 132715.
[21] M.H. Chen, H. Yin, X.Y. Li, Y.P. Qiu, G.X. Cao, J.J. Wang, X.F. Yang, P. Wang, Facet- and defect-engineered Pt/Fe_2O_3 nanocomposite catalyst for catalytic oxidation of airborne formaldehyde under ambient conditions, J. Hazard. Mater. 395 (2020), 122628.
[22] J.W. Ye, M.H. Zhou, Y. Le, B. Cheng, J.G. Yu, Three-dimensional carbon foam supported MnO_2/Pt for rapid capture and catalytic oxidation of formaldehyde at room temperature, Appl. Catal. B-Environ. 267 (2020), 118689.
[23] I.E. Wachs, Catalysis science of supported vanadium oxide catalysts, Dalton T 42 (2013) 11762–11769.
[24] K.I. Otake, Y. Cui, C.T. Buru, Z. Li, J.T. Hupp, O.K. Farha, Single-atom-based vanadium oxide catalysts supported on metal-organic frameworks: Selective alcohol oxidation and structure-activity relationship, J. Am. Chem. Soc. 140 (2018) 8652–8656.
[25] H. Huang, B. Jiang, L. Gu, Z. Qi, H. Lu, Promoting effect of vanadium on catalytic activity of Pt/Ce-Zr-O diesel oxidation catalysts, J. Environ. Sci. 33 (2015) 135–142.
[26] L.J. Jiang, Q.C. Liu, G.J. Ran, M. Kong, S. Ren, J. Yang, J.L. Li, V_2O_5-modified Mn-Ce/AC catalyst with high SO_2 tolerance for low-temperature NH_3-SCR of NO, Chem. Eng. J. 370 (2019) 810–821.
[27] Z. Wu, V. Schwartz, M. Li, A.J. Rondinone, S.H. Overbury, Support shape effect in metal oxide catalysis: Ceria-nanoshape-supported vanadia catalysts for oxidative dehydrogenation of isobutane, J. Phys. Chem. Lett. 3 (2012) 1517–1522.
[28] K. Chen, N. Liu, M.H. Zhang, D.H. Wang, Oxidative desulfurization of dibenzothiophene over monoclinic VO_2 phase-transition catalysts, Appl. Catal. B-Environ. 212 (2017) 32–40.
[29] M.V. Ganduglia-Pirovano, C. Popa, J. Sauer, H. Abbott, A. Uhl, M. Baron, D. Stacchiola, O. Bondarchuk, S. Shaikhutdinov, H.J. Freund, Role of ceria in oxidative dehydrogenation on supported vanadia catalysts, J. Am. Chem. Soc. 132 (2010) 2345–2349.
[30] H. Huang, Y.F. Gu, J. Zhao, X.Y. Wang, Catalytic combustion of chlorobenzene over VO_x/CeO_2 catalysts, J. Catal. 326 (2015) 54–68.
[31] P. Yang, J. Li, Z. Cheng, S. Zuo, Promoting effects of Ce and Pt addition on the destructive performances of V_2O_5/γ-Al_2O_3 for catalytic combustion of benzene, Appl. Catal. A-Gen. 542 (2017) 38–46.
[32] Q.Y. Wang, K.L. Yeung, M.A. Banares, Operando Raman-online FTIR investigation of ceria, vanadia/ceria and gold/ceria catalysts for toluene elimination, J. Catal. 364 (2018) 80–88.
[33] R.S.G. Ferreira, P.G.P. de Oliveira, F.B. Noronha, The effect of the nature of vanadium species on benzene total oxidation, Appl. Catal. B-Environ. 29 (2001) 275–283.
[34] A.Q. Pan, H.B. Wu, L. Yu, X.W. Lou, Template-free synthesis of VO_2 hollow microspheres with various interiors and their conversion into V_2O_5 for lithium-ion batteries, Angew. Chem. Int. Ed. 52 (2013) 2226–2230.
[35] Z. He, X. Wang, Y. Pu, Z. Qian, Fundamental understanding of the role of potassium on the activity of Pt/CeO_2 for the hydrogen production from ethanol, Int. J. Hydrog. Energ. 37 (2012) 11132–11140.
[36] B.Y. Bai, J.H. Li, Positive effects of K^+ ions on three-dimensional mesoporous Ag/Co_3O_4 catalyst for HCHO oxidation, ACS Catal. 4 (2014) 2753–2762.
[37] H.G. Peng, J.W. Ying, J. Zhang, X.H. Zhang, C. Peng, C. Rao, W.M. Liu, N. Zhang, X. Wang, La-doped Pt/TiO_2 as an efficient catalyst for room temperature oxidation of low concentration HCHO, Chin. J. Catal. 38 (2017) 39–47.
[38] Q.C. Li, S.F. Chen, Z.Y. Liu, Q.Y. Liu, Combined effect of KCl and SO_2 on the selective catalytic reduction of NO by NH_3 over V_2O_5/TiO_2 catalyst, Appl. Catal. B-Environ. 164 (2015) 475–482.
[39] Y. Chen, Z. Shao, Y. Yang, S. Zhao, Y. Tao, H. Yao, H. Luo, X. Cao, P. Jin, Electrons-donating derived dual-resistant crust of VO_2 nano-particles via ascorbic acid treatment for highly stable smart windows applications, ACS Appl. Mater. Inter. 11 (2019) 41229–41237.
[40] Z.J. Mei, Y. Li, M.H. Fan, L. Zhao, J. Zhao, Effect of the interactions between Pt species and ceria on Pt/ceria catalysts for water gas shift: the XPS studies, Chem. Eng. J. 259 (2015) 293–302.
[41] G.F. Long, X.H. Li, K. Wan, Z.X. Liang, J.H. Piao, P. Tsiakaras, Pt/CN-doped electrocatalysts: superior electrocatalytic activity for methanol oxidation reaction and mechanistic insight into interfacial enhancement, Appl. Catal. B-Environ. 203 (2017) 541–548.
[42] X.Q. Yang, X.L. Yu, M.Y. Lin, M.F. Ge, Y. Zhao, F.Y. Wang, Interface effect of mixed phase Pt/ZrO_2 catalysts for HCHO oxidation at ambient temperature, J. Mater. Chem. A 5 (2017) 13799–13806.
[43] C.Y. Wang, Y.B. Li, L.R. Zheng, C.B. Zhang, Y. Wang, W.P. Shan, F.D. Liu, H. He, A nonoxide catalyst system study: alkali metal-promoted Pt/AC catalyst for formaldehyde oxidation at ambient temperature, ACS Catal. 11 (2021) 456–465.
[44] Z.X. Yan, Z.H. Xu, J.G. Yu, M. Jaroniec, Enhanced formaldehyde oxidation on CeO_2/AlOOH-supported Pt catalyst at room temperature, Appl. Catal. B-Environ. 199 (2016) 458–465.
[45] Q. Li, Z. Yan, N. Wang, Z. Xu, G. Wang, G. Huang, 0D/2D CeO_2 quantum dot/NiO nanoplate supported an ultralow-content Pt catalyst for the efficient oxidation of formaldehyde at room temperature, Catal. Sci. Technol. 10 (2020) 4030–4041.
[46] S.Q. Song, S.J. Jiang, R.C. Rao, H.X. Yang, A.M. Zhang, Bicomponent VO_2-defects/MWCNT catalyst for hydroxylation of benzene to phenol: promoter effect of defects on catalytic performance, Appl. Catal. A-Gen. 401 (2011) 215–219.
[47] R. Camposeco, S. Castillo, M. Hinojosa-Reyes, V. Rodriguez-Gonzalez, N. Nava, I. Mejia-Centeno, Pt-V_2O_5/NT and Pt-WO_3/NT titanate nanotubes with strong photocatalytic activity under visible light, ChemistrySelect 4 (2019) 1023–1030.
[48] W. Zhao, K. Zhang, L.C. Wu, Q. Wang, D.H. Shang, Q. Zhong, Ti^{3+} doped V_2O_5/TiO_2 catalyst for efficient selective catalytic reduction of NO_x with NH_3, J. Colloid Interf. Sci. 581 (2021) 76–83.
[49] T. Yang, Y. Huo, Y. Liu, Z. Rui, H. Ji, Efficient formaldehyde oxidation over nickel hydroxide promoted Pt/γ-Al_2O_3 with a low Pt content, Appl. Catal. B-Environ. 200 (2017) 543–551.
[50] F. Liu, J. Shen, D.F. Xu, W.Y. Zhou, S.Y. Zhang, L. Wan, Oxygen vacancies enhanced HCHO oxidation on a novel $NaInO_2$ supported Pt catalyst at room temperature, Chem. Eng. J. 334 (2018) 2283–2292.
[51] W.J. Bao, H.X. Chen, H. Wang, R.D. Zhang, Y. Wei, L.R. Zheng, Pt nanoparticles supported on N/Ce-doped activated carbon for the catalytic oxidation of formaldehyde at room temperature, ACS Appl. Nano Mater. 3 (2020) 2614–2624.
[52] S. Aranifard, S.C. Ammal, A. Heyden, Nature of Ptn/CeO_2 (111) surface under water-gas shift reaction conditions: a constrained ab initio thermodynamics study, J. Phys. Chem. C. 116 (2012) 9029–9042.
[53] S.C. Ammal, A. Heyden, Understanding the nature and activity of supported platinum catalysts for the water-gas shift reaction: from metallic nanoclusters to alkali-stabilized single-atom cations, ACS Catal. 9 (2019) 7721–7740.
[54] Y. Xu, A.V. Ruban, M. Mavrikakis, Adsorption and dissociation of O_2 on Pt-Co and Pt-Fe alloys, J. Am. Chem. Soc. 126 (2004) 4717–4725.
[55] S.A. Park, H. Lim, Y.T. Kim, Enhanced oxygen reduction reaction activity due to electronic effects between Ag and Mn_3O_4 in alkaline media, ACS Catal. 5 (2015) 3995–4002.
[56] H.Y.F. Sim, J.R.T. Chen, C.S.L. Koh, H.K. Lee, X. Han, G.C. Phan-Quang, J.Y. Pang, C.L. Lay, S. Pedireddy, I.Y. Phang, E.K.L. Yeow, X.Y. Ling, ZIF-induced d-band modification in a bimetallic nanocatalyst: achieving over 44 % efficiency in the ambient nitrogen reduction reaction, Angew. Chem. Int. Ed. 59 (2020) 16997–17003.